


Article

Displacement Monitoring of a Bridge Based on BDS Measurement by CEEMDAN–Adaptive Threshold Wavelet Method

Chunlan Mo ¹, Huanyu Yang ², Guannan Xiang ¹, Guanjun Wang ¹ , Wei Wang ¹, Xinghang Liu ³ and Zhi Zhou ^{4,*}

¹ School of Information and Communication Engineering, Hainan University, Haikou 570228, China

² Faculty of Infrastructure Engineering, Dalian University of Technology, Dalian 116024, China

³ School of Computer Science and Technology, Hainan University, Haikou 570228, China

⁴ College of Civil Engineering and Architecture, Hainan University, Haikou 570228, China

* Correspondence: zhizhou@hainanu.edu.cn

Abstract: From the viewpoint of BDS bridge displacement monitoring, which is easily affected by background noise and the calculation of a fixed threshold value in the wavelet filtering algorithm, which is often related to the data length. In this paper, a data processing method of Complete Ensemble Empirical Mode Decomposition with Adaptive Noise (CEEMDAN), combined with adaptive threshold wavelet de-noising is proposed. The adaptive threshold wavelet filtering method composed of the mean and variance of wavelet coefficients of each layer is used to de-noise the BDS displacement monitoring data. CEEMDAN was used to decompose the displacement response data of the bridge to obtain the intrinsic mode function (IMF). Correlation coefficients were used to distinguish the noisy component from the effective component, and the adaptive threshold wavelet de-noising occurred on the noisy component. Finally, all IMF were restructured. The simulation experiment and the BDS displacement monitoring data of Nanmao Bridge were verified. The results demonstrated that the proposed method could effectively suppress random noise and multipath noise, and effectively obtain the real response of bridge displacement.

Keywords: beidou navigation system (BDS); bridge monitoring; complete ensemble empirical mode decomposition with adaptive noise (CEEMDAN); adaptive threshold wavelet; data noise reduction



Citation: Mo, C.; Yang, H.; Xiang, G.; Wang, G.; Wang, W.; Liu, X.; Zhou, Z. Displacement Monitoring of a Bridge Based on BDS Measurement by CEEMDAN–Adaptive Threshold Wavelet Method. *Sensors* **2023**, *23*, 4268. <https://doi.org/10.3390/s23094268>

Academic Editor: Branko Glisic

Received: 17 March 2023

Revised: 21 April 2023

Accepted: 22 April 2023

Published: 25 April 2023



Copyright: © 2023 by the authors. Licensee MDPI, Basel, Switzerland. This article is an open access article distributed under the terms and conditions of the Creative Commons Attribution (CC BY) license (<https://creativecommons.org/licenses/by/4.0/>).

1. Introduction

Bridges are a vital component of the road infrastructure network and the development of the national economy. During operation, bridges may be affected by factors such as traffic loads, wind, and earthquakes, resulting in a certain amount of deformation of the bridge. In severe cases, it can lead to safety accidents. Therefore, it is necessary to monitor the health of bridges, especially the displacement generated by the bridge under load [1]. In addition to strain gauge [2], optical fiber sensor, and accelerometer [3], there are also precise level, robotic total station (RTS) [4–9], LiDAR DTMs [10,11], and global navigation satellite system (GNSS) instrument [12–14], etc. Strain gauge and optical fiber sensors have limitations in displacement measurement [1], and the calculation of accelerometer by double integration will lead to serious errors [15,16]. Although level and RTS have achieved good results in displacement monitoring, there are still some limitations, such as not working all day as well as the need to see between stations [12,17,18]. In contrast, as a geodetic survey method, GNSS technology has the advantages of providing three-dimensional coordinates, all-weather operation, and not requiring a line-of-sight between target points [13,14]. As early as 1997, GPS had been applied to the Humber Bridge, and the dynamic displacement of the bridge was successfully obtained [19], indicating that GPS could be applied to bridge monitoring. With the development of GNSS technology, its application in bridge displacement monitoring had also been greatly developed, such as with the application

of GNSS technology in the Talkha highway steel bridge in Mansoura [20], the Yeongjong Grand Bridge in South Korea [21], and the Severn Suspension Bridge in the UK [22]. A large amount of literature has been published in recent years, but most of the research is on GPS [20,23]. Beidou Navigation Satellite System (BDS) is a satellite navigation system that has been formally networked in 2020, and has also been applied in the field of deformation monitoring [24,25]. In terms of bridge displacement monitoring, Xi et al., demonstrated through experiments that the performance of BDS-RTK in bridge monitoring is comparable to that of GPS-RTK, and BDS-RTK is subjected to less background noise [26]. This indicates the feasibility of BDS in bridge displacement monitoring.

When using GNSS for bridge displacement monitoring, due to environmental influences, GNSS signals may contain some noise, such as satellite multipath effects, random noise, etc. [27–29]. The impact of these noises will submerge the true displacement information of the bridge, leading to a decrease in the accuracy of bridge health monitoring. Therefore, it is necessary to find an appropriate method to filter these noises. Most traditional signal processing methods focus on signals with periodic stationarity, while the results of GNSS monitoring signals are nonlinear and non-stationary [30], which includes true displacement information of bridges, errors caused by multipath effects, and random noise [11]. Empirical mode decomposition (EMD) [31] and wavelet analysis [32] are two commonly used and effective methods to process nonlinear and non-stationary signals. Variational Mode Decomposition (VMD) has a good application effect in the signal processing of bridge displacement monitoring due to its unique advantages [33]. However, CiveraM et al., noted in their study that the VMD method is not applicable to non-stationary signals and has certain limitations, while the EMD is more suitable for non-stationary signals [34]. Mode aliasing will occur when a signal is decomposed by EMD [35]. Although EEMD can greatly eliminate modal mixing by adding white noise to EMD, the added noise cannot be completely removed [36]. CEEMDAN proposed by Torres et al. [37] is an improved CEEMD [38] with adaptive noise, which can achieve an accurate recombination of decomposed signals and effectively solve the problem of modal mixing. The CEEMDAN filtering method is used to remove components containing noise directly, but there would still be some effective information in the components, which would be lost if discarded directly. In order to avoid this situation, the EMD method, combined with other data processing methods, has been applied in GNSS signal de-noising. Therefore, Gao et al., used the Hilbert-Huang transform (HHT) and EEMD analysis methods to study the time-frequency characteristics of GNSS strain time series before the Yunnan earthquake, which could better analyze the change characteristics of seismic signals at different scales [39]. Wei et al., combined EEMD with independent component analysis (PSR-ICA) based on phase space reconstruction to analyze the vertical time series of GNSS reference stations and effectively separate independent atmospheric and soil moisture load signals [40]. Wen Chen et al., proposed a method combining the Chebyshev filter and CEEMDAN (CF-CEEMDAN) to de-noise GNSS monitoring signals of offshore platforms [41].

As a classical multi-scale analysis method, wavelet analysis plays an important role in GNSS signal noise reduction [42–44]. In addition to using wavelet analysis alone to process GNSS signals, the GNSS signals are also filtered jointly with the empirical mode decomposition method to solve the detail loss caused by empirical mode decomposition method. For example, RuiRao et al., proposed to use EMD combined with wavelet analysis to de-noise bridge GNSS monitoring and correctly extract bridge frequency [45]. However, this algorithm is affected by the problem of mode mixing in EMD. Niu et al., proposed that EEMD combined the wavelet packet method for dynamic analysis of suspension bridges, and proved that the proposed EEMDWP method was proved to be better than the single EEMD or WP method [46]. Guo et al., proposed a filtering method combining EEMD and wavelet analysis to separate multipath effects in GNSS data [47]. Xiong et al., used CEEMDAN combined with wavelet transform [48] or wavelet packet [30] to conduct noise reduction processing on GNSS-RTK monitoring data of bridges and high-rise buildings. Although the noise reduction method of empirical mode decomposition combined with

wavelet analysis solved the problem of detail information loss to a certain extent, the filtering effect of wavelet analysis method depended on the selection of wavelet basis function, decomposition layers, and threshold. The selection of threshold is usually a fixed threshold or a threshold parameter based on a large amount of experience, which had certain subjectivity. Different threshold selection had different noise reduction effects.

Based on the above analysis, in order to correctly identify the bridge displacement, change in the BDS displacement monitoring signal containing noise, and to reduce the influence of subjectivity of threshold selection in wavelet de-noising, a method combining CEEMDAN and adaptive threshold wavelet (CEEMDAN-AWT) is proposed in this paper to reduce the noise of bridge BDS monitoring signal. The Section 2 introduces the method of data collection in this paper. In Section 3, the principle of this method is introduced and the performance of this method is evaluated by using analog signal. In Section 4, firstly, the stability of the BDS receiver is tested, and the noise reduction effect of the proposed method on the measured data is evaluated. Finally, the monitoring signals of bridge engineering are applied and the monitoring results of bridge displacement are analyzed.

2. Data Collection Method

The equipment used for data collection in this paper is the split GNSS receiver M900SE provided by Sinan Navigation Company, as shown in Figure 1. The antenna is an AT60 antenna, which can simultaneously observe the entire galaxy (GPS, GLONASS, Galileo, BDS) satellite. The receiver is equipped with a 4G transmission module, which can upload the collected data to the cloud server in real time through the wireless network. Simultaneously, it is also equipped with an RS232 serial port, which can transmit the data through the wired way, which allows the data collection to be more comprehensive and convenient. The data collection flow chart is shown in Figure 2.



Figure 1. Main equipment of data collection: (a) M900SE receiver; (b) AT60 antenna.

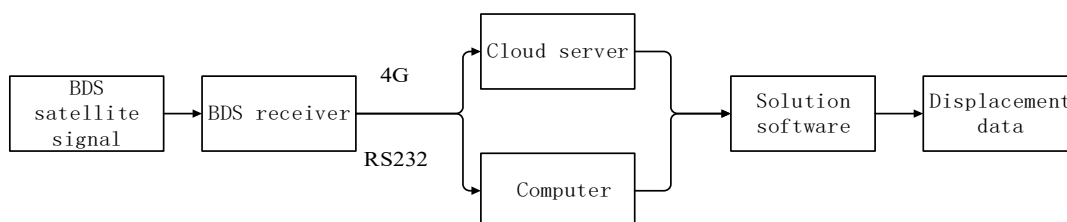


Figure 2. Data collection flow chart.

The steps of data collection are as follows:

1. A BDS receiver is used to receive signals from BDS satellites.

The observation method adopted in this paper is relative positioning technique [14]. Relative positioning refers to the joint observation of the satellite by the reference station and the monitoring station. The coordinates of the reference station are usually known by

certainty, and then the coordinates of the monitoring station are determined by calculating the baseline vector between the reference station and the monitoring station. This occurs as shown in Figure 3.

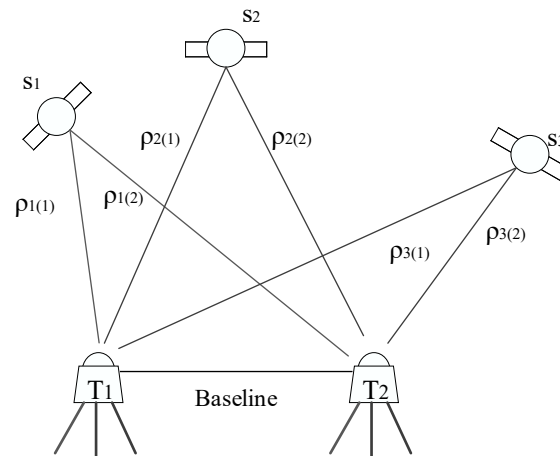


Figure 3. Relative positioning work diagram.

In Figure 3, S1–S3 represent the satellites. T1 and T2 are two receiving devices, one of which serves as the reference station and the other as the monitoring station.

2. After processing the received satellite signal, the receiving device transmits it to the cloud server through the 4G network or to the upper computer through an RS232 serial port.
3. The collected satellite data is relative computed with the commercial software compass solution to obtain the three-dimensional coordinates of the monitoring station, and then the displacement time series is obtained through the Equation (1) [21].

$$\begin{bmatrix} \Delta x_i \\ \Delta y_i \\ \Delta z_i \end{bmatrix} = \begin{bmatrix} x_i \\ y_i \\ z_i \end{bmatrix} - \frac{1}{n} \sum_{i=0}^{i=n} \begin{bmatrix} x_i \\ y_i \\ z_i \end{bmatrix} \quad (1)$$

where $(\Delta x_i, \Delta y_i, \Delta z_i)$ is the displacement of each recorded moment (epoch), n is the total number of epochs, $i = 1, 2, 3$.

3. Principle of CEEMDAN-Adaptive Threshold Wavelet Algorithm

This section introduces the basic theory and workflow of CEEMDAN-adaptive threshold wavelet (CEEMDAN-AWT) method and tests the method with analog signals. Firstly, the signal is decomposed by the CEEMDAN method, and the noisy component and effective component are distinguished by the correlation coefficients between each component and the signal. Then, adaptive threshold wavelet de-noising is carried out on the noisy component to retain more details of the signal. Finally, all components are reconstructed.

3.1. CEEMDAN Algorithm

Adaptive noise complete set Empirical Mode decomposition (CEEMDAN) is an improved algorithm for the EMD [31] algorithm and EEMD [36] algorithm with mode aliasing and residual white noise in components. The CEEMDAN decomposition steps of bridge monitoring signal $y(t)$ [37] are as follows:

1. A new signal $y'(t) = y(t) + (-1)^q \varepsilon v^j(t)$ is obtained by adding Gaussian white noise to $y(t)$.

where $q = 1, 2$, ε is the standard deviation of white noise, $v^j(t)$ is the Gaussian white noise signal, N is the number of times white noise is added, $j = 1, 2, \dots$. After EMD de-

composition of the new signal, the first order characteristic mode component C_1 of EMD decomposition is obtained.

$$E\left(y(t) + (-1)^q \varepsilon v^j(t)\right) = C_1^j(t) + r^j \quad (2)$$

where the function $E(y(t) + (-1)^q \varepsilon v^j(t))$ represents the EMD decomposition process, $C_1^j(t)$ is the first order eigenmode component of EMD decomposition, and r^j is the residual of EMD decomposition.

2. The first modal component IMF_1 of CEEMDAN decomposition is obtained by an overall averaging of the N modal components generated:

$$IMF_1 = \overline{C_1(t)} = \frac{1}{N} \sum_{j=1}^N C_1^j(t) \quad (3)$$

where N is the number of first-order modal components decomposed by EMD.

3. Remove the first modal component to obtain the first residual of the signal:

$$r_1(t) = y(t) - IMF_1 \quad (4)$$

where $y(t)$ is the original signal added with white noise and IMF_1 is the first-order modal component of CEEMDAN.

4. A new signal $r_1'(t)$ is obtained by adding white Gaussian noise to $r_1(t)$, and then the signal is decomposed by EMD to obtain the first mode component D_1 of $r_1'(t)$, and the second eigenmode component IMF_2 is obtained by averaging:

$$IMF_2 = \overline{C_2(t)} = \frac{1}{N} \sum_{j=1}^N D_1^j(t) \quad (5)$$

where N is the number of first-order modal components decomposed by EMD, and $D_1^j(t)$ is the first-order modal components decomposed by signal $r_1'(t)$.

5. After removing the second modal component, the second residual $r_2(t)$ of signal $y(t)$ is obtained:

$$r_2(t) = r_1(t) - IMF_2 \quad (6)$$

where $r_1(t)$ is the first residual of the signal $y(t)$ and IMF_2 is the second CEEMDAN modal component of the signal $y(t)$.

6. Repeat the above steps until the obtained residual signal is a monotone function, then the decomposition is complete. At this point, the signal $y(t)$ is decomposed into K modal components and a residual component:

$$y(t) = \sum_{k=1}^K IMF_k + r_t(t) \quad (7)$$

where K is the number of modal components, IMF_k is the K th modal component, and $r_t(t)$ is the residual component of signal $y(t)$.

It can be seen from Equation (7) that bridge displacement monitoring signal $y(t)$ can be decomposed into K modal components and one residual term. The CEEMDAN method directly removes the noise component to realize signal de-noising.

3.2. Adaptive Threshold Wavelet Algorithm

The CEEMDAN method directly removes the noisy component, but will lose some details of the signal. In contrast, the wavelet threshold de-noising method is de-noising

the signal through the limit of the threshold. Therefore, wavelet threshold de-noising can retain more effective information in the noisy component. The specific methods of wavelet threshold de-noising for noisy components are as follows:

1. Select the appropriate wavelet basis function and the appropriate number of decomposition layers.
2. Quantify the high-frequency decomposition layer with a threshold value.
3. All wavelet coefficients are reconstructed to obtain de-noised signals.

In the above steps, the selection of threshold is the key link in wavelet threshold de-noising. Common thresholds include an unbiased risk estimation threshold, fixed threshold, heuristic threshold, and minimax threshold [42], among which the fixed threshold is widely used in GNSS signal de-noising, and can be presented as follows [45]:

$$\lambda = \sigma \sqrt{2 \ln N} \sigma = \frac{\text{median}(|cd1|)}{0.6745} \quad (8)$$

where σ is noise variance, N is signal length, and $cd1$ is the detail coefficient of the first layer decomposition [45].

According to Equation (8), the fixed threshold is not only related to noise variance, but also to signal length. If the signal is too long or too short, the de-noising effect will be weakened to some extent. In view of the above situation, this paper proposes an adaptive threshold calculation method, and can be presented as follows:

$$\lambda = \mu_j + \max(cd_j) * \delta_j \quad j = 1, 2, \dots, k \quad (9)$$

where μ is the mean value, δ is the variance of the wavelet coefficients of this layer, respectively, and j is the number of decomposition layers. The threshold calculation method is to adaptively select the high frequency coefficients of each layer to avoid the influence of data length on the threshold and all wavelet coefficients use the same threshold filtering.

3.3. CEEMDAN-Adaptive Threshold Wavelet Algorithm Process

The noise reduction process of CEEMDAN-AWT method is shown in Figure 4. The specific process is as follows:

1. The original signal was decomposed into each order modal component (IMF component) and a residual component (res component) by CEEMDAN.
2. Calculate the correlation coefficients r between IMF components of each order and the original signal [30], and it can be presented as follows:

$$r = \frac{\sum_i^N (y[i] - \bar{y})(IMF[i] - \overline{IFM})}{\sqrt{\sum_i^N (y[i] - \bar{y})^2 (IMF[i] - \overline{IFM})^2}} \quad (10)$$

where y is the original data, \bar{y} is the average value, IMF is the modal components of each order, and \overline{IFM} is the average value. The IMF component with the first local minimum of the correlation coefficient is selected as the boundary, the IMF component from the first IMF component to this IMF component is the noise component, and the remaining components are the effective components.

3. The noisy components are de-noised by the wavelet threshold and quantized by the soft threshold function [45]. The soft threshold function is as follows:

$$w_\lambda = \begin{cases} \text{sgn}(w) * (|w| - \lambda) & |w| \geq \lambda \\ 0 & |w| < \lambda \end{cases} \quad (11)$$

where w is each wavelet coefficient, λ is the critical threshold, and $\text{sgn}(x)$ is a symbolic function.

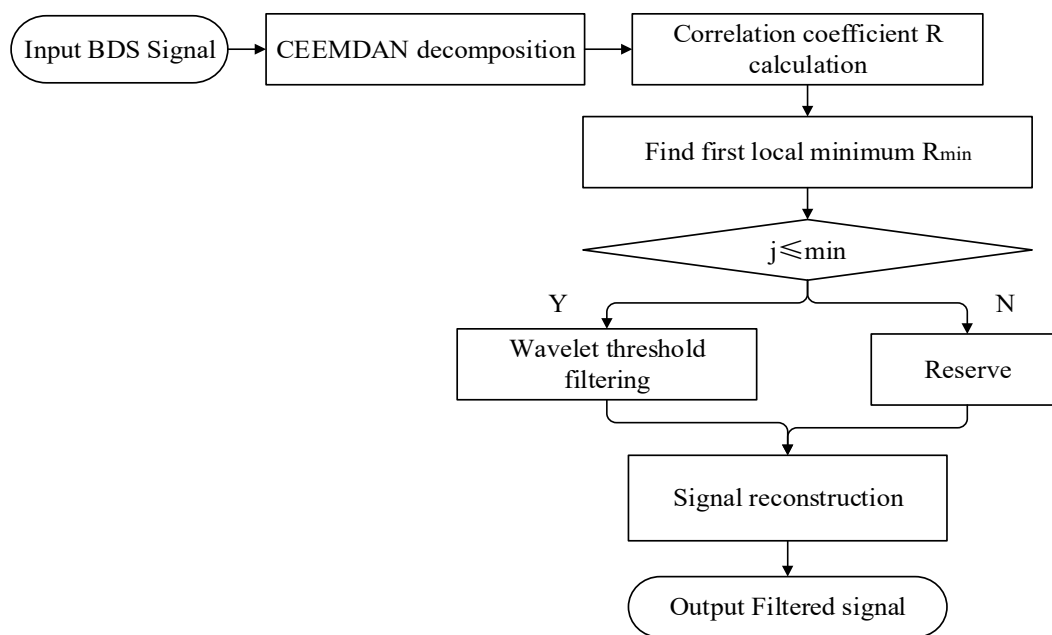


Figure 4. Flow chart of noise reduction.

4. The filtered IMF components was reconstructed.

In order to evaluate the noise reduction performance of the noise reduction method, signal-to-noise ratio (SNR) and root mean square error (RMSE) are introduced [30]. As follows:

$$SNR = 10 \log_{10} \frac{\sum_i^N y(i)^2}{\sum_i^N [y(i) - y'(i)]^2} \quad (12)$$

$$RMSE = \sqrt{\frac{1}{N} \sum_i^N [y(i) - y'(i)]^2} \quad (13)$$

where $y(t)$ is the original data, $y'(t)$ is the data after noise removal, and N is the data length. The larger the SNR or the smaller the RMSE denotes the better the noise reduction effect.

3.4. Performance Evaluation of CEEMDAN-Adaptive Threshold Wavelet Algorithm

To evaluate the performance of CEEMDAN-AWT method, $y(t) = 5\sin(2\pi * 0.7t) + 7\sin(2\pi * 0.5t) + n(t)$ was used as the analog signal in this paper. The signal consists of sinusoidal signals with frequency of 0.7 Hz and 0.5 Hz and random noise $n(t)$. The sampling frequency of the analog signal is 100 Hz. Figure 5 shows the images of signal without noise and signal $y(t)$ with 5 dB noise added.

By comparing Figure 5a,b, it can be seen that after adding noise, the signal appears burr and the signal smoothness is weakened, indicating that noise will affect the correct recognition and use of the signal, therefore, it needs to be processed by filtering. After CEEMDAN of $y(t)$, 11 IMF components and 1 residual component were shown in Figure 6. Equation (10) was used to calculate the correlation coefficients between each IMF component and $y(t)$, as shown in Table 1.

It can be seen from Table 1 that the first locally minimum IMF component of the correlation coefficient was IMF4, as such it was determined that IMF1~IMF4 were noise components, while IMF5~IMF11 were effective components. The comparison between the reconstructed signal and $y(t)$ after processing by using the CEEMDAN-AWT method proposed in this paper is shown in Figure 7.

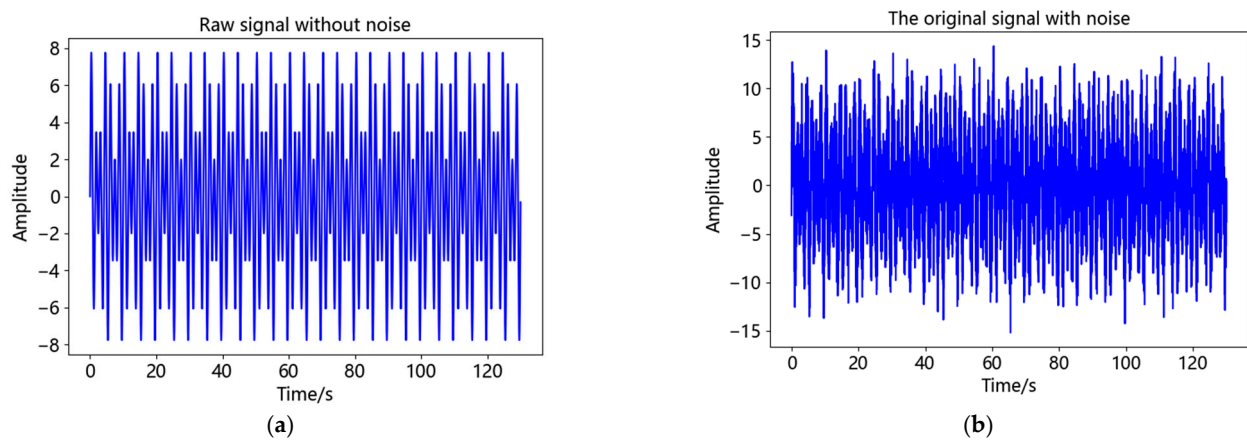


Figure 5. Amplitudes of $x(t)$ and $y(t)$: (a) Amplitudes of $x(t)$; (b) Amplitudes of $y(t)$.

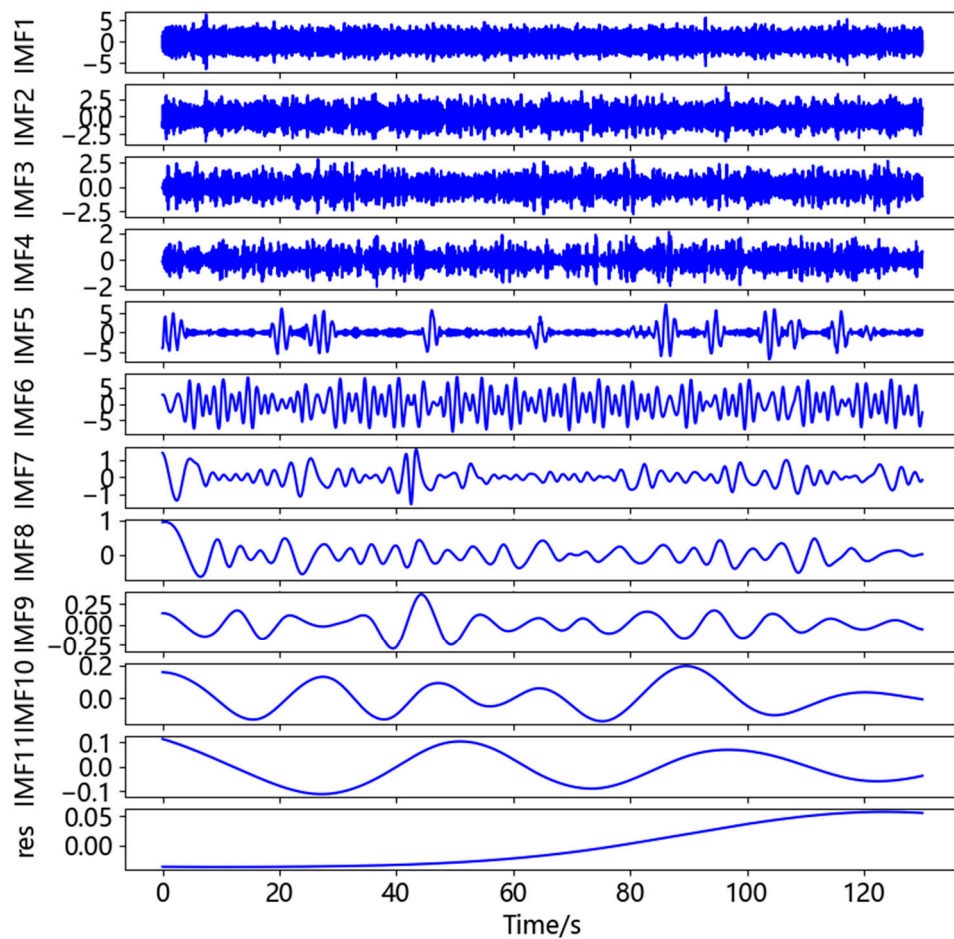


Figure 6. CEEMDAN decomposition of $y(t)$.

Table 1. Correlation coefficients between IMF components and $y(t)$.

IMF No.	IMF1	IMF2	IMF3	IMF4	IMF5	IMF6	IMF7	IMF8	IMF9	IMF10	IMF11
Correlation coefficients	0.357	0.211	0.168	0.109	0.321	0.838	0.229	0.025	0.013	0.012	−0.014

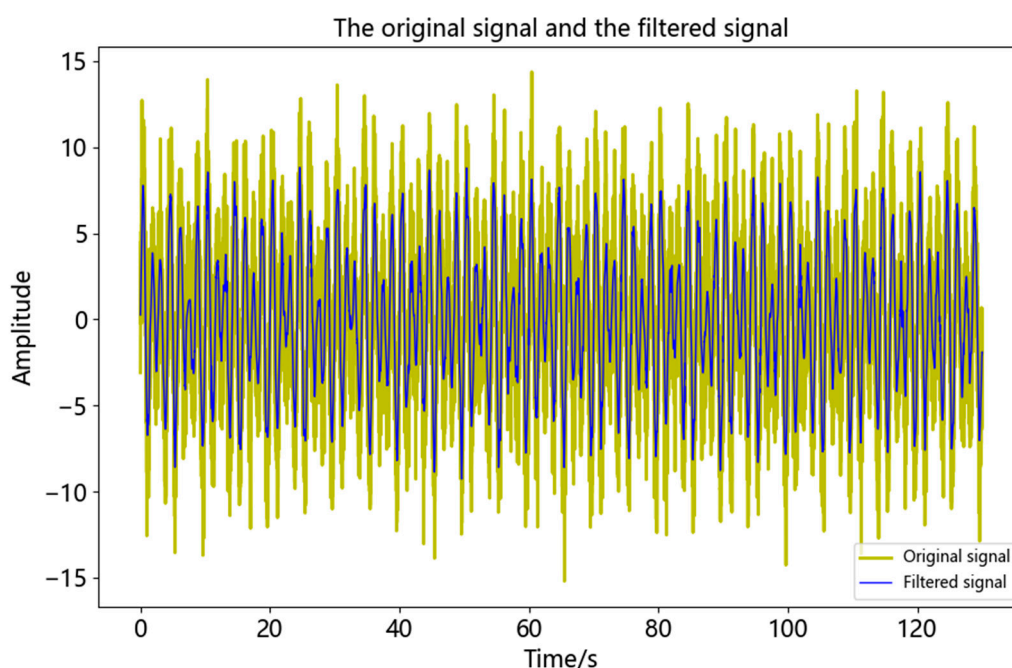


Figure 7. Comparison between the analog signal and the original signal after noise reduction.

It can be seen from Figure 7 that after filtering, the signal was smoother and less sharp, which was more similar to $x(t)$ and retained the details of the signal. In order to evaluate the noise reduction effect of the proposed method, it was compared with the CEEMDAN method and CEEMDAN-fixed threshold wavelet (CEEMDAN-FWT) method, respectively. The evaluation indexes calculated according to Equations (12) and (13) were shown in Table 2. In Table 2, noise signals at different signal-to-noise ratio levels (5 dB, 10 dB, 15 dB, 20 dB, and 25 dB) were also compared and analyzed.

Table 2. Evaluation indicators of analog signal noise reduction.

Different Noise Levels	5 dB		10 dB		15 dB		20 dB		25 dB	
	SNR/dB	RMSE/mm	SNR/dB	RMSE/mm	SNR/dB	RMSE/mm	SNR/dB	RMSE/mm	SNR/dB	RMSE/mm
CEEMDAN	6.356	2.271	10.662	1.265	15.368	0.715	20.609	0.386	25.539	0.218
CEEMDAN-FWT	6.360	2.269	10.698	1.260	15.527	0.702	20.891	0.374	26.030	0.206
CEEMDAN-AWT	6.377	2.265	10.786	1.247	15.857	0.676	22.410	0.314	30.188	0.127

It can be seen from Table 2 that the SNR and RMSE of the signal processed by CEEMDAN-AWT method were the maximum and the minimum. This indicates that the performance of the CEEMDAN-AWT method was better than the other two methods and was more suitable for the suppression of random noise in BDS monitoring signals.

4. Experimental Results and Discussion

4.1. Background Noise Analysis

In order to evaluate the background noise of the receiver, two M900SE GNSS receivers of Sinan Navigation were used for static test in an open square. The experimental test Figure 8 was as follows. One receiver was used as the reference station and the other as the monitoring station. The two devices were used for synchronous data acquisition with a sampling frequency of 1 Hz and a total test time of 3 h and 33 min. The length of the baseline between the two stations was 4.06 m, which was classified as a short baseline (<5 km) [49]. Both sensors were stationary. Theoretically, the displacement of the monitoring station should have been zero. Therefore, the non-zero results in the test were visually generated by the background noise. The solution software was used to solve the collected BDS satellite signals, and the displacement time series was calculated according to Equation (1), as

shown in Figure 9. The displacement time series included horizontal direction (north-south direction and east-west direction; N-S direction and E-W direction) and vertical direction (U direction). The mathematical statistical characteristics of the displacement time series in the three directions are shown in Table 3.



Figure 8. Background noise test system diagram.

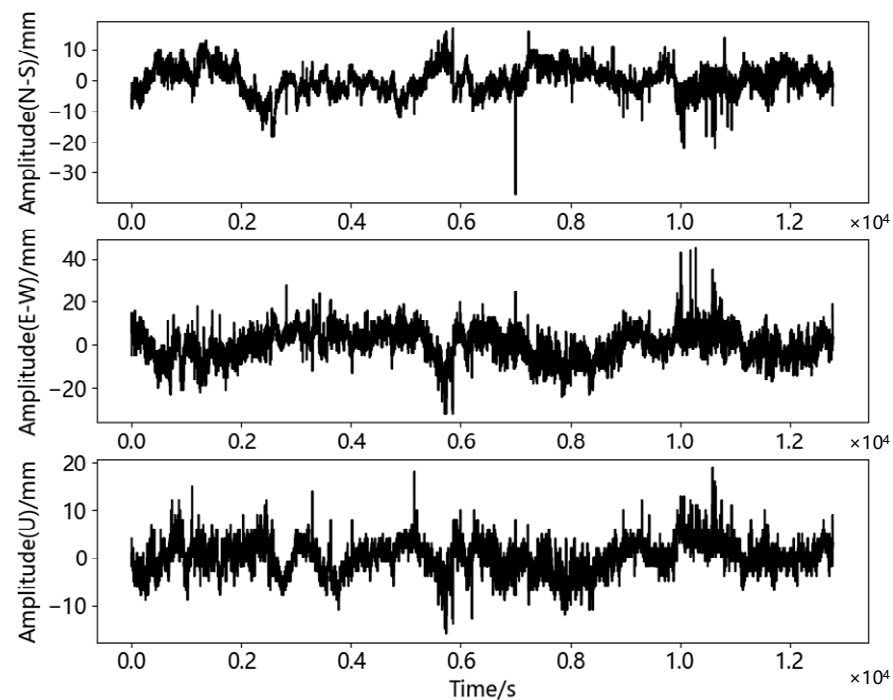


Figure 9. Three direction original time series of the BDS static test.

Table 3. Basic information of the original time series.

Signal	Mean/mm	Std/mm	Max/mm	Min/mm
N-S direction	5.4180×10^{-8}	4.3992	16.926	−37.074
E-W direction	-9.0183×10^{-7}	7.0044	44.883	−32.117
U direction	-5.1194×10^{-8}	5.4179	19.080	−15.920

It can be seen from Figure 9 and Table 3 that the displacement data of the three directions were mainly concentrated near zero, in which the maximum value of the N-S direction was 16.926 mm and the minimum value was −37.074 mm; the maximum value of the E-W direction was 44.883 mm and the minimum value was −32.117 mm. The maximum value of the U direction was 19.080 mm and the minimum value was −15.920 mm. It can be seen from the Figure 9 that the maximum value occupied a small proportion column in

the whole signal and did not appear continuously, and thus it was determined that there may have been gross error in this time series. In order to judge and remove gross errors, the commonly used 3σ criterion method was introduced, which was as follows [50]:

1. Calculate the average \bar{X} of displacement time series, as shown in Equation (14).

$$\bar{X} = \frac{1}{n} \sum_{i=1}^n X_i \quad (14)$$

where \bar{X} is the mean value of the displacement time series, n is the sequence length, and X_i is the displacement at every moment.

2. The residual error v_i of the sequence is calculated as shown in Equation (15).

$$v_i = X_i - \bar{X} \quad (15)$$

where X_i is the displacement at every moment, and \bar{X} is the mean value of the displacement time series.

3. Calculate the root mean square deviation, σ , of the sequence according to Bessel method, as shown in Equation (16).

$$\sigma = \sqrt{\sum v_i^2 / (n - 1)} \quad (16)$$

where v_i is the residual of the monitoring data sequence and n is the length of the sequence.

4. Judge according to the above results. If $|X_i - \bar{X}| > 3\sigma$, X_i will be judged as gross error and removed, and the average value will be used for interpolation; otherwise, X_i will be judged as normal value and retained.

After removing coarse error, the horizontal displacement ranged from $-12.074 \sim 11.926$ mm in the north-south direction and from $-20.117 \sim 19.883$ mm in the east-west direction. The vertical displacement was $-8.920 \sim 9.080$ mm. The accuracy of the BDS sensor used in this study was ± 10 mm in the horizontal direction and ± 15 mm in the vertical direction. The displacement generated by environmental noise exceeded the measurement range in the horizontal direction, while in the vertical direction, although it did not exceed the measurement accuracy, it could be seen from the figure that there were some fluctuations and burrs in the displacement time series, which still indicated that the measurement by BDS sensor would be affected by noise. The displacement time series was processed by CEEMDAN-AWT filtering. Figure 10 demonstrated the IMF components of displacement time series in three directions. The correlation coefficients, r , of each IMF component and each displacement time series were calculated, respectively, as shown in Table 4.

According to Table 4, the correlation coefficient 0.125 of IMF5 in the north-south direction was the first local minimum, while the first local minimum of the correlation coefficient in the east-west direction and the vertical direction was IMF4, which was 0.178 and 0.204, respectively. Therefore, in the N-S direction IMF1-IMF5 were noise components and IMF6-IMF11 were effective components. In the E-W and U directions IMF1-IMF4 were noise components and IMF5-IMF11 were effective components. The comparison between the filtered displacement time series and the original displacement time series was shown in Figure 11. As can be seen from Figure 11, after noise reduction the time series became smoother, the sharp points were suppressed, and the data accuracy was also improved. Under static observation after noise reduction, the displacement range in the N-S direction was $-9.915 \sim 11.180$ mm, the displacement range in the E-W direction was $-15.856 \sim 15.833$ mm, and the displacement range in the U direction was $-7.409 \sim 7.780$ mm. It can be seen that in addition to the east-west direction, the measurement accuracy of the instrument was satisfied in the north-south direction and the vertical direction. Under the influence of the multipath effect, the accuracy of the U direction was still less than 8mm, which could meet the needs of bridge monitoring.

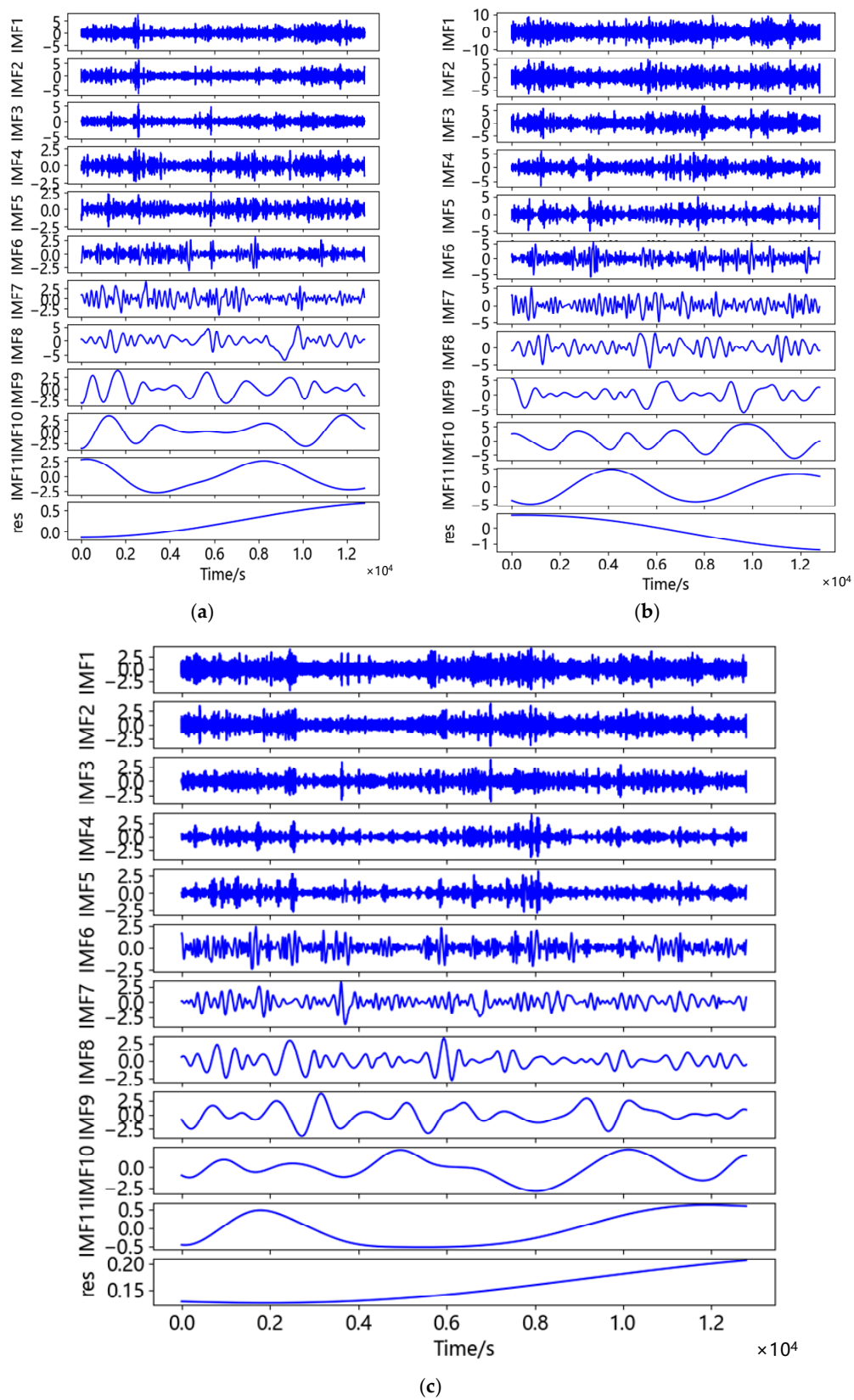
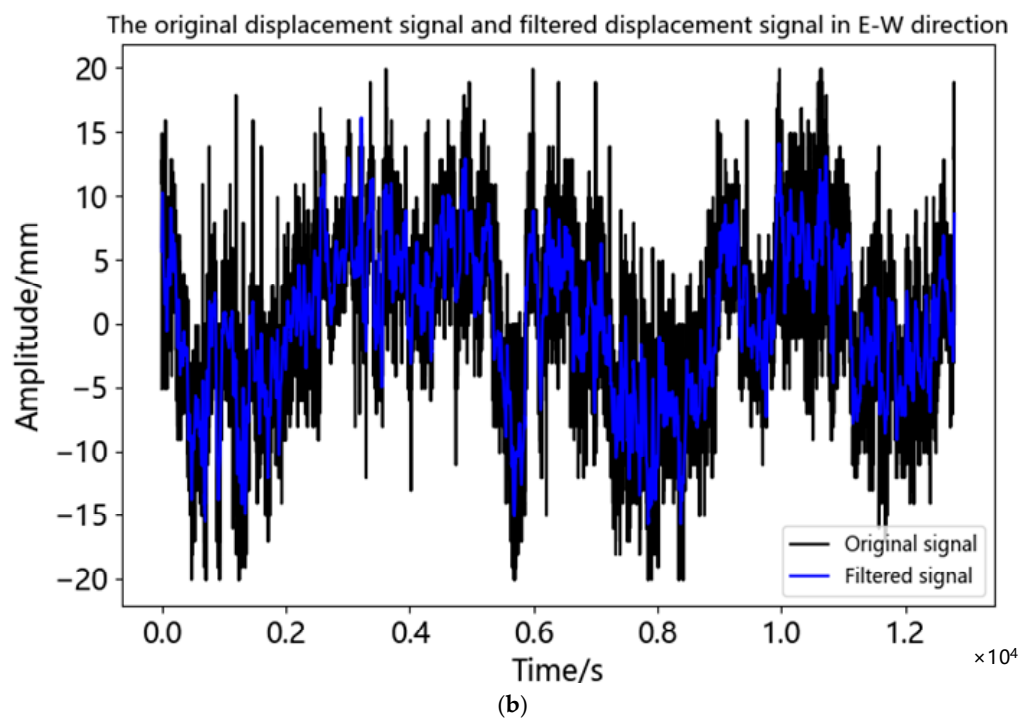
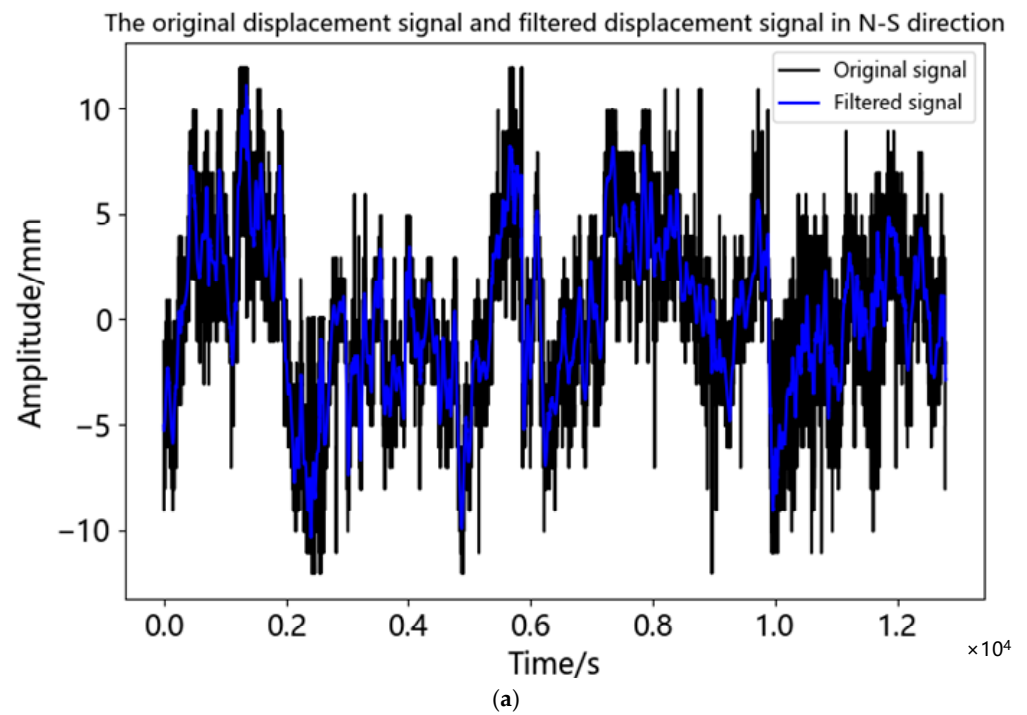


Figure 10. CEEMDAN decomposition of data in three directions: (a) CEEMDAN decomposition of data in N-S direction; (b) CEEMDAN decomposition of data in E-W direction; (c) CEEMDAN decomposition of data in U direction.

Table 4. Correlation coefficients between IMF and original signals in three directions.

Signal	Correlation Coefficients										
	IMF1	IMF2	IMF3	IMF4	IMF5	IMF6	IMF7	IMF8	IMF9	IMF10	IMF11
N-S direction	0.256	0.182	0.162	0.151	0.125	0.239	0.334	0.415	0.520	0.404	0.371
E-W direction	0.324	0.220	0.206	0.178	0.193	0.256	0.264	0.252	0.311	0.432	0.523
U direction	0.308	0.229	0.209	0.204	0.208	0.215	0.219	0.347	0.525	0.271	0.342

**Figure 11.** Cont.

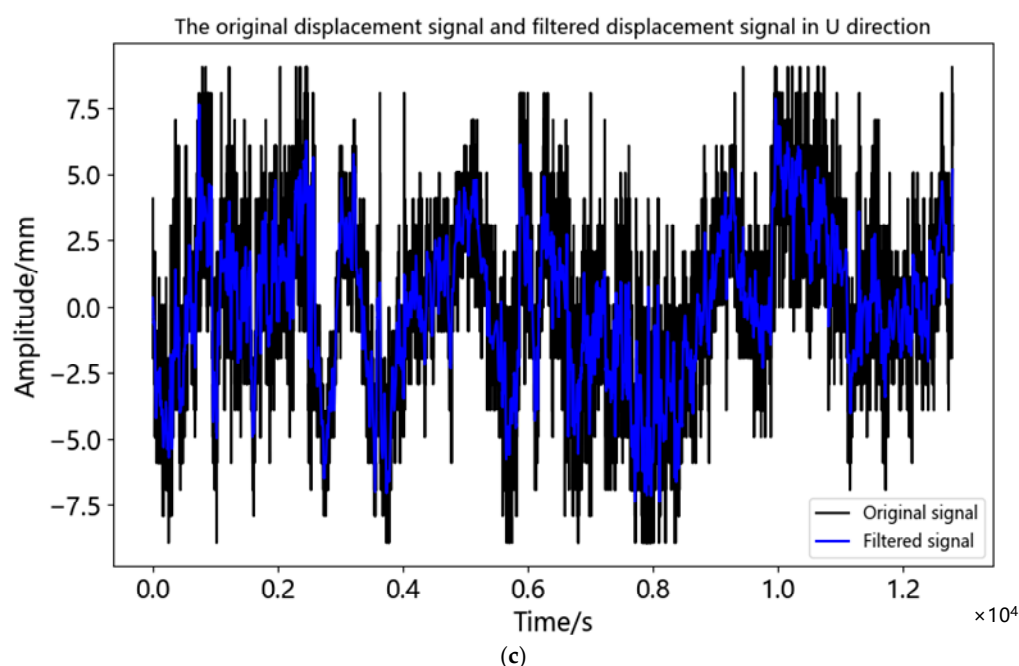


Figure 11. Comparison of original and de-noised signals in three directions of static test experiment: (a) Comparison of original and de-noised signals in N-S direction; (b) Comparison of original and de-noised signals in E-W direction; (c) Comparison of original and de-noised signals in U direction.

In order to evaluate the noise reduction effect of the proposed method on static test data, it was compared with the CEEMDAN method and the CEEMDAN-FWT method, then the evaluation indexes of the three methods were calculated using Equations (12) and (13), as shown in Table 5.

Table 5. Noise reduction performance of different methods.

Signal	N-S Direction		E-W Direction		U Direction	
	SNR/dB	RMSE/mm	SNR/dB	RMSE/mm	SNR/dB	RMSE/mm
CEEMDAN	7.424	1.761	6.317	3.268	6.327	1.568
CEEMDAN-FWT	7.453	1.755	6.321	3.266	6.349	1.564
CEEMDAN-AWT	7.472	1.751	6.325	3.265	6.393	1.556

It can be seen from Table 5 that SNR of the CEEMDAN-AWT method for displacement time series de-noising in three directions in a static test was the largest among the three methods, while RMSE was the smallest among the three methods. This meant that the performance of the CEEMDAN-AWT method in actual measurement data was better than the other two algorithms.

4.2. De-Noising of Bridge BDS Displacement Measurement Signal

A field survey was carried out in Nanmaoqiao, Baoting Autonomous County, Hainan Province. The length of Nanmao bridge was 260.68 m. The main bridge was 127.0 m long and 15 m wide, which was a highway bridge connecting Baoting County and Nanmao Farm. The bridge was the only way for people to travel and purchase farm, and the traffic flow was relatively large. In this test, a monitoring station was set up at the mid-span position of the bridge, and a reference station was set up on an unopened road 91 m away from the bridge. The coordinates of the reference station were obtained by conventional static positioning method. The instruments used in the test included two split receivers of Sinan M900SE, equipped with power supply equipment and laptop computers. Figure 12 demonstrates the layout of monitoring stations and reference stations in this test. The experiment occurred at 13:00 on 8 December 2022, with a total of five hours of observation.

The sampling frequency of the equipment was 1 Hz, and the cut-off angle of the satellite was 15 degrees. Since the bridge was mainly affected by the traffic volume, this paper only analyzed the time series in the vertical (U) direction. Figure 13 showed the displacement time series diagram in the vertical direction of this test. Table 6 showed the basic statistical characteristics of bridge monitoring data.



(a)



(b)



(c)

Figure 12. Layout diagram of bridge testing sensors: (a) Sensor's layout diagram (background image from Baidu Maps); (b) Reference station; (c) Monitoring station.

After calculation, the maximum value and minimum value of the data obtained in this experiment was 28.969 mm and −46.031 mm. However, as shown in Figure 13, these data occupy relatively few specific columns throughout the entire time series and were not clustered. Therefore, it was determined that there was a coarse error in the displacement

time series, and the 3σ method performed coarse error processing on the original data. The baseline length between the two stations in this test was 91 m, which was considered a short baseline. The satellite clock deviation and receiver clock deviation could be eliminated through relative positioning, and the atmospheric propagation delay could be ignored [50]. The main source of error in the displacement time series was the random noise received by the device during reception. The displacement time series after gross error removal was decomposed by CEEMDAN, and the IMF components were shown in Figure 14. The correlation coefficient, r , of each IMF component and displacement time series was calculated according to Equation (10), as shown in Table 7.

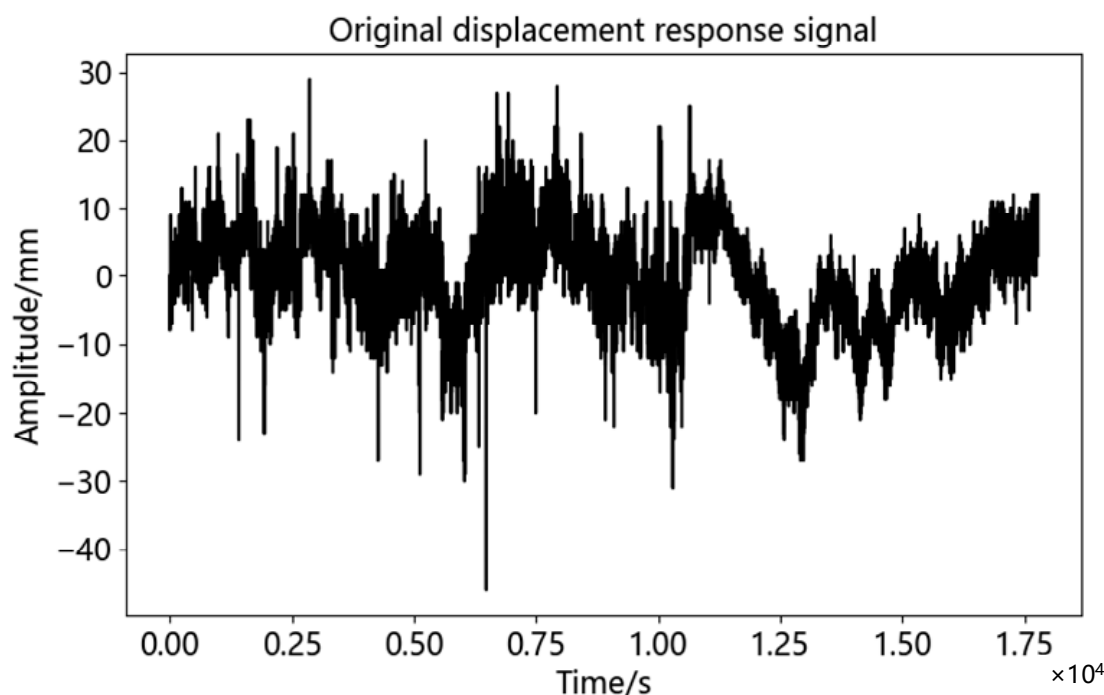


Figure 13. Original time series of elevation displacement.

Table 6. Basic statistical characteristics of bridge monitoring data.

Signal	Mean/mm	Std/mm	Max/mm	Min/mm
U dir	-1.869×10^{-12}	6.872	28.969	-46.031

As can be seen from Table 7, the first local minimum of correlation coefficient was IMF5, and its correlation coefficient with displacement time series was 0.145. Therefore, IMF~IMF5 was judged as the noise component, and IMF6~IMF12 as the effective component. The adaptive threshold wavelet de-noising was carried out for IMF1~IMF5 and reconstructed with the effective component. The comparison between the filtered displacement time series and the original displacement time series was shown in Figure 15. In order to further evaluate the noise reduction effect of the proposed method on displacement time series, the CEEMDAN method and the CEEMDAN-FWT method were carried out on displacement time series at the same time, and their evaluation indexes were calculated and shown in Table 8.

As shown in Table 8, after noise reduction by the CEEMDAN-AWT method, SNR of displacement time series was 7.186 dB, which was the largest among the three methods, and RMSE was 2.884 mm, which was the smallest among the three methods. This meant that the noise reduction effect of the proposed method was better than that of the other two methods, which was consistent with the simulation results.

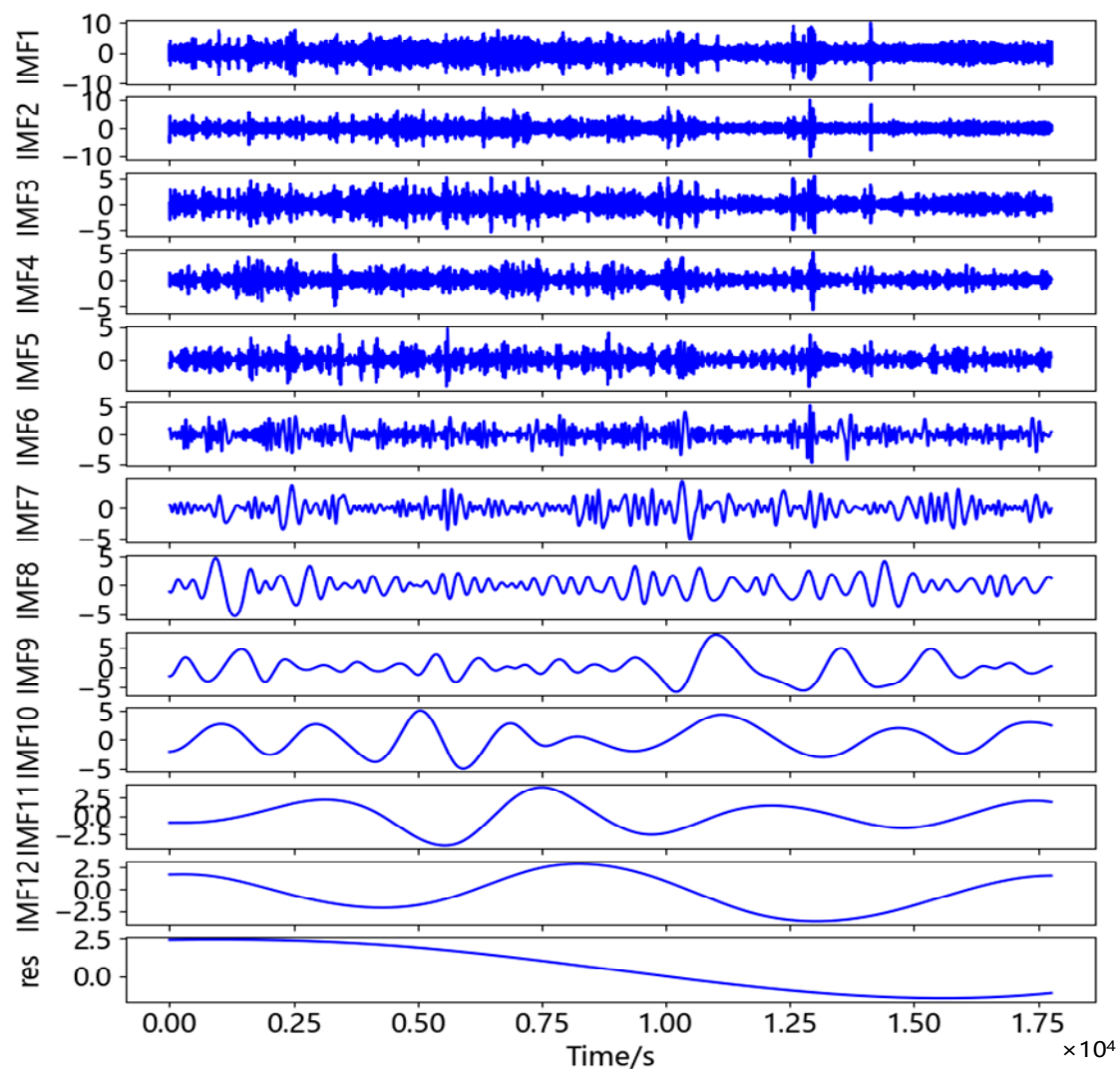


Figure 14. CEEMDAN decomposition diagram in U direction of Nanmao Bridge dynamic test.

Table 7. Correlation coefficient between IMF and original signal.

IMF No.	IMF1	IMF2	IMF3	IMF4	IMF5	IMF6
Correlation coefficients	0.279	0.190	0.171	0.152	0.145	0.155
IMF No.	IMF7	IMF8	IMF9	IMF10	IMF11	IMF12
Correlation coefficients	0.150	0.247	0.272	0.535	0.545	0.481

It can be seen from Figure 15 that the displacement time series became smoother and less sharp after de-noising. The correlation coefficient between the calculated filtered displacement time series and the original displacement time series was 0.899. The higher correlation meant that more details of the displacement response of the bridge were preserved, which can better reflect the deformation information of the bridge. According to Figure 15, the maximum value of displacement time series after noise reduction was 13.595 mm and the minimum value was -16.179 mm. The period of maximum displacement was about 12.500 s to 15.000 s in the time series, which was from 16:00 to 18:00 of the day. During this period, it was the peak time of commuting and the traffic volume was relatively large.

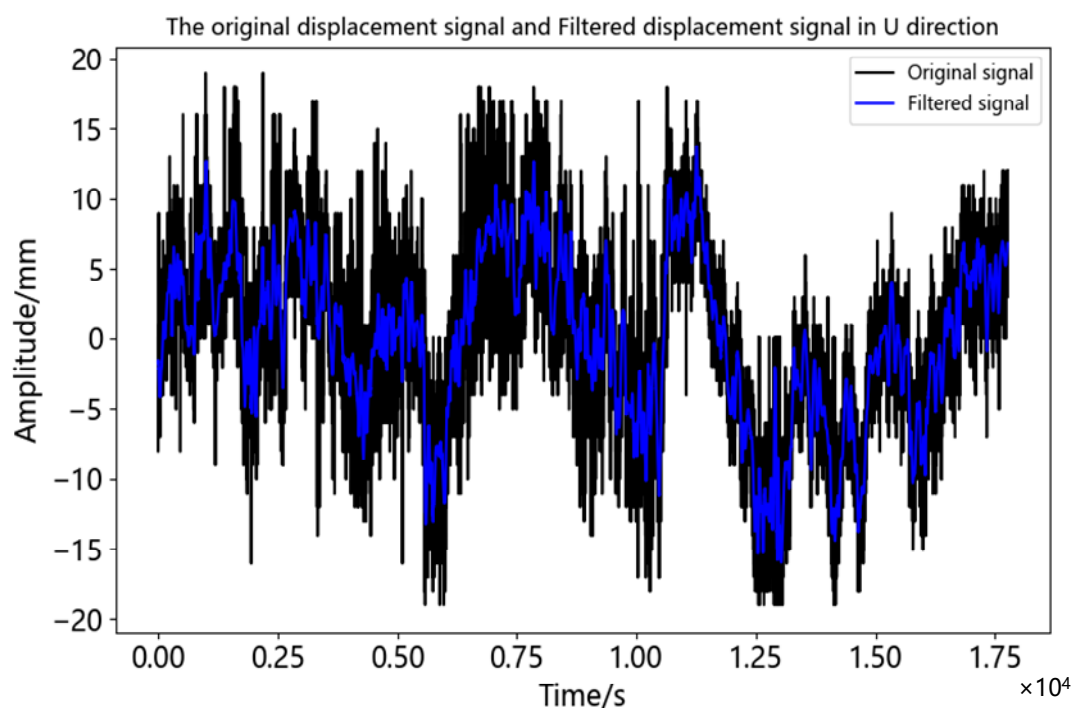


Figure 15. Comparison of the original signal and de-noised signal of bridge displacement monitoring.

Table 8. Noise reduction performance of different methods of bridge monitoring signal.

Indicator	Method		
	CEEMDAN	CEEMDAN-FWT	CEEMDAN-AWT
SNR/dB	7.175	7.177	7.186
RMSE/mm	2.888	2.887	2.884

5. Conclusions

In this paper, a CEEMDAN-AWT method is proposed to solve the problem that the monitoring data of bridge displacement monitoring by BDS technology will be submerged due to the influence of background noise. The following conclusions are obtained through the test:

Through the SNR and RMSE analysis of three proposed methods of CEEMDAN, CEEMDAN-FWT method, and CEEMDAN-AWT method for a series of analog signals with different SNR levels, it is found that the CEEMDAN-AWT method has a better noise reduction effect than other two methods. It can be used to improve the precision of BDS displacement monitoring.

The stability test data of BDS receiver is processed by the CEEMDAN-AWT method. After noise reduction, the SNR of the north-south signal is 7.472 dB and RMSE of 1.751 mm, and the SNR of east-west signal is 6.325 dB and RMSE of 3.265 mm. The SNR and RMSE of vertical signal were 6.393 dB and 1.556 mm, respectively. The random noise of the three direction monitoring signals is suppressed. In the horizontal direction, the measuring range of the north-south direction is $-9.915\sim 11.180$ mm, and the measuring range of the east-west direction is $-15.856\sim 15.833$ mm, which is still higher than the measuring accuracy of the instrument after filtering, so it is necessary to seek a better method for processing. The measurement range in the vertical direction is $-7.409\sim 7.780$ mm, which meets the monitoring requirements in the vertical direction of the bridge.

After using the proposed CEEMDAN-AWT method to reduce bridge data, the SNR is 7.186 dB and RMSE is 2.884 mm, and the noise reduction effect is better than the other two methods. The correlation coefficient between the filtered monitoring data and the original monitoring data is 0.899, which effectively preserves the detailed information of

the displacement monitoring response signal. During the monitoring period, the maximum displacement change of -16.179 mm occurred under the traffic load. This method provides an excellent noise reduction method for bridge deformation monitoring, but it is a pity that the dynamic response of the bridge cannot be analyzed deeply due to the limitation of sampling frequency of experimental instruments.

Author Contributions: Conceptualization, C.M.; methodology, C.M., H.Y., Z.Z. and G.W.; validation, C.M., G.X. and X.L.; formal analysis, C.M. and W.W.; writing—original draft preparation, C.M.; writing—review and editing, C.M., W.W., H.Y. and Z.Z.; supervision, Z.Z. and G.W.; All authors have read and agreed to the published version of the manuscript.

Funding: 1. Hainan Provincial Natural Science Foundation High-level Talents Project (2019RC097). 2. Key Consulting Project of the Chinese Academy of Engineering (20-HN-XZ-03) 3. Innovative Research Project of Graduate Students in Hainan Province (Qhys2021-45). Authors give cordial thanks for these funding organizations.

Institutional Review Board Statement: Not applicable.

Informed Consent Statement: Not applicable.

Data Availability Statement: The authors confirm that the data supporting the findings of this study are available within the article.

Conflicts of Interest: The authors declare no conflict of interest.

Abbreviations

CEEMDAN: Complete Ensemble Empirical Mode Decomposition with Adaptive Noise; BDS: beidou navigation system; GNSS: global navigation satellite system; GPS: Global Positioning System; GLONASS: Global Navigation Satellite System; Galileo: Galileo satellite navigation system; IMF: intrinsic mode function; CEEMDAN-AWT: A method combining CEEMDAN and adaptive threshold wavelet; CEEMDAN-FWT: A method combining CEEMDAN and fix threshold wavelet; SNR: signal-to-noise ratio; RMSE: root mean square error.

References

1. Moschas, F.; Stiros, S. Measurement of the dynamic displacements and of the modal frequencies of a short-span pedestrian bridge using GPS and an accelerometer. *Eng. Struct.* **2011**, *33*, 10–17. [\[CrossRef\]](#)
2. Boštjan, K.; Rok, K.; Andrej, Š.; Nikolai, V. Processing of Signals Produced by Strain Gauges in Testing Measurements of the Bridges. *Procedia Eng.* **2015**, *117*, 795–801. [\[CrossRef\]](#)
3. Fenerci, A.; Øiseth, O.; Rønquist, A. Long-term monitoring of wind field characteristics and dynamic response of a long-span suspension bridge in complex terrain. *Eng. Struct.* **2017**, *147*, 269–284. [\[CrossRef\]](#)
4. Moschas, F.; Psimoulis, P.A.; Stiros, S.C. GPS/RTS data fusion to overcome signal deficiencies in certain bridge dynamic monitoring projects. *Smart Struct. Syst.* **2013**, *12*, 251–269. [\[CrossRef\]](#)
5. Ante, M.; Rinaldo, P.; Domagoj, D. Measurement of bridge dynamic displacements and natural frequencies by RTS. *Grđevinar* **2019**, *4*, 281–294. [\[CrossRef\]](#)
6. Samo, L.; Boštjan, K. A Comparative Study of Signal Processing Methods for Contactless Geodetic Monitoring. *Appl. Sci.* **2021**, *11*, 11276. [\[CrossRef\]](#)
7. Kovacic, B.; Mursec, L.; Lubej, S. Synchronisation of contactless vibration monitoring methods. *Int. J. Simul. Model. (IJSIMM)* **2022**, *21*, 113–123. [\[CrossRef\]](#)
8. Kovačič, B.; Mursec, L.; Toplak, S.; Lubej, S. Non-contact monitoring for assessing potential bridge damages. *E3S Web Conf.* **2020**, *164*, 3001. [\[CrossRef\]](#)
9. Alojz, K.; Imrich, L.; Peter, K.; Ján, E. Dynamic deformation monitoring of a technological structure. *Geod. List* **2013**, *67*, 161–174.
10. Mahmoud, A.M.A.; Hussain, E.; Novellino, A.; Psimoulis, P.; Marsh, S. Monitoring the Dynamics of Formby Sand Dunes Using Airborne LiDAR DTMs. *Remote Sens.* **2021**, *13*, 4665. [\[CrossRef\]](#)
11. Kim, K.; Kim, J. Dynamic displacement measurement of a vibratory object using a terrestrial laser scanner. *Meas. Sci. Technol.* **2015**, *26*, 045002. [\[CrossRef\]](#)
12. Wang, X.P.; Zhao, Q.Z.; Xi, R.J.; Li, C.F.; Li, G.Q.; Li, L. Review of Bridge Structural Health Monitoring Based on GNSS: From Displacement Monitoring to Dynamic Characteristic Identification. *IEEE Access* **2021**, *9*, 1. [\[CrossRef\]](#)

13. Yi, T.H.; Li, H.N.; Gu, M. Recent research and applications of GPS-based monitoring technology for high-rise structures. *Struct. Control. Health Monit.* **2013**, *20*, 649–670. [\[CrossRef\]](#)
14. Shen, N.; Chen, L.; Liu, J.B.; Wang, L.; Tao, T.Y.; Wu, D.W.; Chen, R.Z. A review of global navigation satellite system (GNSS)-based dynamic monitoring technologies for structural health monitoring. *Remote Sens.* **2019**, *11*, 1001. [\[CrossRef\]](#)
15. Yang, J.; Li, J.; Lin, G. A simple approach to integration of acceleration data for dynamic soil-structure interaction analysis. *Soil Dyn. Earthq. Eng.* **2006**, *26*, 725–734. [\[CrossRef\]](#)
16. Stiros, S.C. Errors in velocities and displacements deduced from accelerographs: An approach based on the theory of error propagation. *Soil Dyn. Earthq. Eng.* **2008**, *28*, 415–420. [\[CrossRef\]](#)
17. Zarikas, V.; Gikas, V.; Kitsos, C. Evaluation of the Optimal Design “cosinor model” for Enhancing the Potential of Robotic Theodolite Kinematic Observations. *Measurement* **2010**, *43*, 1416–1424. [\[CrossRef\]](#)
18. Yi, T.H.; Li, H.N.; Gu, M. Experimental assessment of high-rate GPS receivers for deformation monitoring of bridge. *Measurement* **2013**, *46*, 420–432. [\[CrossRef\]](#)
19. Ashkenazi, V.; Roberts, W. Experimental Monitoring of the Humber Bridge Using GPS. In *Civil Engineering*; Thomas Telford—ICE Virtual Library: London, UK, 1997; Volume 120, pp. 177–182. [\[CrossRef\]](#)
20. Nickitopoulou, A.; Protopsalti, K.; Stiros, S. Monitoring dynamic and quasi-static deformations of large flexible engineering structures with GPS: Accuracy, limitations and promises. *Eng. Struct.* **2006**, *28*, 1471–1482. [\[CrossRef\]](#)
21. Elnabwy, M.T.; Kaloop, M.R.; Elbeltagi, E. Talkha steel highway bridge monitoring and movement identification using RTK-GPS technique. *Measurement* **2013**, *46*, 4282–4292. [\[CrossRef\]](#)
22. Kim, K.Y.; Choi, J.; Chung, J.Y.; Koo, G.H.; Bae, I.-H.; Sohn, H. Structural displacement estimation through multi-rate fusion of accelerometer and RTK-GPS displacement and velocity measurements. *Measurement* **2018**, *130*, 223–235. [\[CrossRef\]](#)
23. Kaloop, M.R.; Hussan, M.; Kim, D. Time-series analysis of GPS measurements for long-span bridge movements using wavelet and model prediction techniques. *Adv. Space Res.* **2019**, *63*, 3505–3521. [\[CrossRef\]](#)
24. Jiang, W.P.; Xi, R.J.; Chen, H.; Xiao, Y.G. Accuracy analysis of continuous deformation monitoring using BeiDou Navigation Satellite System at middle and high latitudes in China. *Adv. Space Res.* **2017**, *59*, 843–857. [\[CrossRef\]](#)
25. Roberts, G.W.; Tang, X. The use of PSD analysis on BeiDou and GPS 10 Hz dynamic data for change detection. *Adv. Space Res.* **2017**, *59*, 2794–2808. [\[CrossRef\]](#)
26. Xi, R.J.; Jiang, W.P.; Meng, X.L.; Chen, H.; Chen, Q. Bridge monitoring using BDS-RTK and GPS-RTK techniques. *Measurement* **2018**, *120*, 128–139. [\[CrossRef\]](#)
27. Xiong, C.B.; Lu, H.L.; Zhu, J.S. Operational modal analysis of bridge structures with data from GNSS/accelerometer measurements. *Sensors* **2017**, *17*, 436. [\[CrossRef\]](#) [\[PubMed\]](#)
28. Zheng, D.W.; Zhong, P.; Ding, X.L.; Chen, W. Filtering GPS time-series using a Vondrak filter and cross-validation. *J. Geod.* **2005**, *79*, 363–369. [\[CrossRef\]](#)
29. Moschas, F.; Stiros, S. Noise characteristics of high-frequency, short-duration GPS records from analysis of identical, collocated instruments. *Measurement* **2013**, *46*, 1488–1506. [\[CrossRef\]](#)
30. Xiong, C.B.; Yu, L.N.; Niu, Y.B. Dynamic Parameter Identification of a Long-Span Arch Bridge Based on GNSS-RTK Combined with CEEMDAN-WP Analysis. *Appl. Sci.* **2019**, *9*, 1301. [\[CrossRef\]](#)
31. Tang, D.; Xu, C.C.; Yue, Q.J.; Wu, W.H.; Shi, Z.M.; Feng, J.G. Single point mooring system modal parameter identification based on empirical mode decomposition and time-varying autoregressive model. *Appl. Ocean Res.* **2015**, *53*, 250–256. [\[CrossRef\]](#)
32. Fang, Z.; Yu, J.Y.; Meng, X.L. Modal Parameters Identification of Bridge Structures from GNSS Data Using the Improved Empirical Wavelet Transform. *Remote Sens.* **2021**, *13*, 3375. [\[CrossRef\]](#)
33. Luo, L.F.; Shan, D.S.; Zhang, E.H. Component extraction method for GNSS displacement signals of long-span bridges. *J. Civ. Struct. Health Monit.* **2023**, *13*, 591–603. [\[CrossRef\]](#)
34. Civera, M.; Surace, C. A Comparative Analysis of Signal Decomposition Techniques for Structural Health Monitoring on an Experimental Benchmark. *Sensors* **2021**, *21*, 1825. [\[CrossRef\]](#) [\[PubMed\]](#)
35. Huang, N.E.; Long, S.R.; Wu, M.L.C.; Shih, H.H.; Zheng, Q.N.; Yen, N.C.; Tung, C.C.; Liu, H.H.; Shen, Z. The empirical mode decomposition and the Hilbert spectrum for nonlinear and non-stationary time series analysis. *Proc. R. Soc. Lond. Ser. A Math. Phys. Eng. Sci.* **1998**, *454*, 903–995. [\[CrossRef\]](#)
36. Wu, Z.; Huang, N.E. Ensemble empirical mode decomposition: A noise-assisted data analysis method. *Advances in adaptive data analysis. Adv. Adapt. Data Anal.* **2009**, *1*, 1–41. [\[CrossRef\]](#)
37. Torres, M.E.; Colominas, M.A.; Schlotthauer, G.; Flandrin, P. A complete ensemble empirical mode decomposition with adaptive noise. In Proceedings of the IEEE International Conference on Acoustics, Speech and Signal Processing (ICASSP), Prague, Czech Republic, 22–27 May 2011; pp. 4144–4147. [\[CrossRef\]](#)
38. Yeh, J.R.; Shieh, J.S.; Huang, N.E. Complementary ensemble empirical mode decomposition: A novel noise enhanced data analysis method. *Adv. Adapt. Data Anal.* **2010**, *2*, 135–156. [\[CrossRef\]](#)
39. Gao, H.; Yuan, X.P.; Gan, S.; Zhang, M. Analysis of seismogenic information of GNSS strain time series based on HHT-EEMD method in Yunnan region. *Acta Geod. Cartogr. Sin.* **2022**, *51*, 1899–1910. [\[CrossRef\]](#)
40. Peng, W.; Dai, W.J.; Santerre, R.; Cai, C.S.; Kuang, C.L. GNSS Vertical Coordinate Time Series Analysis Using Single-Channel Independent Component Analysis Method. *Pure Appl. Geophys.* **2017**, *174*, 723–736. [\[CrossRef\]](#)

41. Chen, W.; Xiong, C.B.; Yu, L.N.; Lian, S.D.; Ye, Z. Dynamic monitoring of an offshore jacket platform based on RTK-GNSS measurement by CF-CEEMDAN method. *Appl. Ocean. Res.* **2021**, *115*, 102844. [[CrossRef](#)]
42. Kaczmarek, A.; Kontny, B. Identification of the Noise Model in the Time Series of GNSS Stations Coordinates Using Wavelet Analysis. *Remote Sens.* **2018**, *10*, 1611. [[CrossRef](#)]
43. Oluropo, O.; Jae, K.L.; Gethin, W.R. Wavelet De-noising of GNSS Based Bridge Health Monitoring Data. *J. Appl. Geod.* **2014**, *8*, 273–282. [[CrossRef](#)]
44. Kankanamge, Y.; Hu, Y.F.; Shao, X.Y. Application of wavelet transform in structural health monitoring. *Earthq. Eng. Eng. Vib.* **2020**, *19*, 515–532. [[CrossRef](#)]
45. Rao, R.; Li, C.C.; Huang, Y.H.; Zhen, X.X.; Wu, L.Z. Method for Structural Frequency Extraction from GNSS Displacement Monitoring Signals. *J. Test. Eval.* **2019**, *47*, 2026–2043. [[CrossRef](#)]
46. Niu, Y.B.; Xiong, C.B. Analysis of the dynamic characteristics of a suspension bridge based on RTK-GNSS measurement combining EEMD and a wavelet packet technique. *Meas. Sci. Technol.* **2018**, *29*, 085103. [[CrossRef](#)]
47. Guo, S.S.; Yu, X.W.; Long, F.Y.; Wang, J.F. Combined filter method for weakening GNSS multipath error. *J. Southeast Univ. (Engl. Ed.)* **2022**, *38*, 178–185. [[CrossRef](#)]
48. Xiong, C.B.; Wang, M.; Chen, W. Data analysis and dynamic characteristic investigation of large-scale civil structures monitored by RTK-GNSS based on a hybrid filtering algorithm. *J. Civ. Struct. Health Monit.* **2022**, *12*, 857–874. [[CrossRef](#)]
49. Xi, R.J.; Chen, H.; Meng, X.L.; Jiang, W.P.; Chen, Q. Reliable Dynamic Monitoring of Bridges with Integrated GPS and BeiDou. *J. Surv. Eng.* **2018**, *144*, 04018008. [[CrossRef](#)]
50. Wu, H.; Lu, N.; Zou, J.; Guo, S. An Improved 3σ Gross Error Detection Method for GNSS Deformation Monitoring Time Series. *Geomat. Inf. Sci. Wuhan Univ.* **2019**, *44*, 1282–1288. [[CrossRef](#)]

Disclaimer/Publisher's Note: The statements, opinions and data contained in all publications are solely those of the individual author(s) and contributor(s) and not of MDPI and/or the editor(s). MDPI and/or the editor(s) disclaim responsibility for any injury to people or property resulting from any ideas, methods, instructions or products referred to in the content.